Studies on the 3-Lamellar Morphology of Miktoarm Terpolymers

Hyeyoung Kim[1], Matthias M L Arras[2], J. P. Mahalik[3,4,5], Weiyu Wang[3], Duk Man Yu[1], Sergey Chernyy[6], Monojoy Goswami[3,4], Rajeev Kumar[3,4,5], Bobby G. Sumpter[3,4], Kunlun Hong[3], Gregory S. Smith[2], and Thomas P. Russell[1,7*]

[1]Department of Polymer Science and Engineering, University of Massachusetts, Amherst, 120 Governors Drive, Amherst, Massachusetts 01003, United States

[2]Large Scale Structures Group, Neutron Scattering Division, Oak Ridge National Laboratory, Tennessee 37831, United States

[3]Center for Nanophase Materials Sciences, Oak Ridge National Laboratory, Oak Ridge, Tennessee, 37831, United States

[4]Computational Sciences and Engineering Division, Oak Ridge National Laboratory, Oak Ridge, Tennessee, 37831, United States

[5]Department of Mathematics, University of Tennessee, Knoxville, Tennessee, 37916, United States

[6]Department of Micro- and Nanotechnology, Technical University of Denmark, Produktionstorvet, 2800 Lyngby, Denmark

[7]Beijing Advanced Innovation Center for Soft Matter Science and Engineering, Beijing University of Chemical Technology, Bejing 100029, China

ABSTRACT

The morphologies of ABC miktoarm star terpolymer consisting of polystyrene (PS), polyisoprene (PI), and poly(2-vinylpyridine) (P2VP) (SIV) were studied by combining small angle neutron and X-ray scattering (SANS and SAXS) and transmission electron microscopy (TEM). We find that this system displays a rich phase behavior including an alternate lamellar (ALT.LAM), cylinder in undulated lamellar (CYLULAM), and 3-lamellar (LAM-3) phase. While the SAXS data alone was insufficient to conclusively differentiate between possible phases, we show that the use of selective dueteration and SANS is essential to unambiguously identify the morphology. In particular, the primary peak in SANS for the miktoarm polymer containing deuterated PS was found to be lower than the next two higher order peaks. Such an unusual scattering pattern for a lamellar morphology was justified by the SCFT calculations when the relative strength of the interaction between PI-P2VP over PS-PI is equal or greater than 2 ($\chi_{IV}/\chi_{SI} \geq 2$).

KEYWORDS: Miktoarm polymer, directed self-assembly, small angle neutron scattering, self-consistent field theory.

INTRODUCTION

Block copolymers (BCPs), linking together two or more chemically distinct polymers, can self-assemble into arrays of nanoscopic microdomains that have been used as templates and scaffolds for the fabrication of nanostructured inorganic materials, separations media, and low dielectric constant materials.[1-5] The structure of BCPs can be classified into linear and branched by the location of the junction points connecting the blocks. The morphologies of linear AB BCPs exhibited spherical, cylindrical, lamellar, and gyroid types have been extensively studied due to the relative simplicity of the synthesis, characterization, and theoretical analysis. In ABC BCPs composed of three chemically different homopolymers covalently linked together, the addition of a third block increases the number and complexity of the morphologies, driven primarily by the volume fractions of the components and the relative strength of the segmental interactions between the components. Added to this is the architecture of the chain: whether the three different blocks are sequenced linearly or if the blocks share the same junction point to make a star-type copolymer. Such a star terpolymer is named a miktoarm star block terpolymer if all blocks are different.

In comparison to linear triblock copolymers, there are fewer studies on ABC miktoarm terpolymers, due, in part, to the complexity of the synthesis.[6-9] In addition, the morphological characteristics of ABC miktoarm terpolymers are quite different from those of linear triblock copolymers due to their chain architecture. For instance, in strongly segregated microphase separated melts, the chemical junction points of linear triblock copolymers get confined on a two-dimensional interface between their blocks, while the junction points of ABC miktoarm terpolymers are, in principle, aligned along a line.[10,11] This difference gives rise to tessellated or tiled morphologies not found in the linear analogs.[12-18] Moreover,

hierarchical morphologies with multiple characteristic length scales can be found due to differences in the strengths of interactions between the blocks and/or differences in the molecular masses or volume fractions of the blocks.[14]

Isono and coworkers were the first to study ABC miktoarm terpolymers consisting of three strongly incompatible arms, namely polydimethylsiloxane (PDMS), polystyrene (PS), and poly(tert-butyl methacrylate) (PtBMA).[19] They observed a 3-fold symmetry by TEM and SAXS where the junction points between the three incompatible blocks were confined to a line.[20] Hadjichristidis and coworkers investigated ABC miktoarm terpolymers with PS, polyisoprene (PI), and poly(methyl methacrylate) (PMMA) blocks.[21,22] A two-dimensional periodic microstructure, consisting of an inner PI column with a surrounding PS annulus in a matrix of PMMA (three microphases) were found with the junction points at the interface between PS and PI. Matsushita and coworkers investigated miktoarm terpolymers of PS, PI, and poly(2-vinylpyridine) (P2VP) blocks.[23-26] They meticulously examined the tilings, which had honeycomb-type and 4-fold and 6-fold symmetries, as a function of the volume fraction of each component. Recently, solvent vapor annealing of thin films of ABC miktoarm terpolymers were investigated where morphologies distinct from the bulk morphologies were found due to the constraints placed on the morphologies by the film thickness and interfacial interactions.[27-29]

Theoretical studies on ABC miktoarm terpolymers have focused mainly on the influence of the volume fraction of the three components on the equilibrium morphology[12-14, 30-34] where the segmental interaction parameters were equal for all the three pairs ($\chi_{AB}=\chi_{AC}=\chi_{BC}$, termed symmetric) and for the case where $\chi_{AB}=\chi_{AC}\neq\chi_{BC}$ (termed asymmetric). The asymmetric interaction case has been found to capture the morphological behavior of PS-PI-P2VP miktoarm terpolymers observed experimentally[35] where the P2VP fraction was

varied.[12,14] A gradual transition from Archimedean tilings to hierarchical structures were found as the P2VP volume fraction was increased. There are few studies focusing on the influence of the strength of segmental interactions on the morphology of the miktoarm terpolymers. Huang and coworkers investigated the effect of interaction parameter on the morphology of ABC miktoarm terpolymers with fixed compositions using dissipative particle dynamics simulations.[16] The interaction strength affected the morphology only when the volume fraction of one of the components dominated.

Miktoarm stars based on poly(cis 1,4-isoprene) (I), poly(styrene) (S) and poly(2-vinylpyridine) (V), allowed for systematic studies of the effects of composition, chemical microstructure and temperature on the thermodynamics of microphase separation. For such studies, we have synthesized eleven ISV-x (I:S:V = 1:1:x, v:v:v) miktoarm stars.

Recently, the influence of composition, chemical microstructure, and annealing temperature on the morphology of PS-PI-P2VP miktoarm terpolymer was systematically studied.[36] This study showed a transition in the morphology from lamellae, [8.8.4] tiling, cylinders in undulating lamellae, to hexagonally packed core-shell cylinder phase by increasing the P2VP volume ratio. Despite these advances in understanding the microphase separation in ABC miktoarm terpolymers, characterization of various morphologies using transmission electron microscopy (TEM) and small-angle X-ray and neutron scattering (SAXS and SANS) remains a challenge. TEM image shows the each microdomain by selective staining, but it is limited to examining the local morphology within an area of several square microns. Furthermore, even when symmetry of the morphologies gets established, interpretation of the scattering requires careful investigation of the different contributions from the three components to the scattering. In this work, we present results to characterize morphology in an ABC miktoarm terpolymer containing PS, PI, and P2VP arms,

abbreviated as SIV, having a volume ratio of 1.0:1.3:4.0. We used TEM, SAXS, SANS, and the self-consistent field theory (SCFT) to characterize a lamellar morphology with three microphase separated domains (named LAM-3). The SCFT was used to compute scattering curves and understand the origin of anomalous scattering pattern in SANS for the SIV miktoarm containing deuterated PS. The SCFT calculations not only reproduced the experimentally observed scattering and the TEM images, but also revealed that there are three competing lamellar-like morphologies which can be stabilized based on the ratio of repulsive interaction strengths between different blocks.

EXPERIMENTAL SECTION

Materials. Styrene (Fisher, >99%), styrene-d8 (Aldrich, >98%), 2-vinylpyridine (Aldrich, >98%), isoprene (Fisher, >99%), 2-chlorobutane (Fisher, >99%), hexane (Fisher, >99.5%), methanol (Fisher, >99.9%), benzene (Aldrich, >99.9%), cyclohexane (Fisher, >99%), tetrahydrofuran (Aldrich, >99%), and 1,4-bis(1-phenylvinyl)benzene (PEB, donated by Dow Chemical, >95%) were purified based on previously reported method.[37] Lithium (Aldrich, >99%) and CaH_2 (Aldrich) were used as received. Sec-butyl lithium (sec-BuLi) was prepared by combining 2-chlorobutane with Li metal under vacuum.

Synthesis of ABC Miktoarm Terpolymer. Synthetic procedures and characterization data for all compounds and BCPs are provided in detail in the Supporting Information (SI).

Characterization. ^{1}H NMR spectra were acquired on a Varian Mercury 500 instrument using deuterated chloroform ($CDCl_3$). Molar mass and molecular weight distributions were measured by size exclusion chromatography (SEC) in THF/0.5% triethylamine (TEA) at 40 ^oC with a flow rate of 1.0 ml/min using an Agilent 1260 Infinity HPLC system consisting of a pump, a degasser, an autosampler, an instant pilot controller, a Wyatt TREOS multi-angle

light scattering detector, a Wyatt Optilab rEX differential refractive index detector, and four Phenomenex Phenogel columns in series. Table 1 shows the molar mass and volume fraction of each block in the SIV and SIV with deuterated PS, abbreviated as dSIV.

Table 1. The molar mass and volume fraction of each block for SIV and dSIV miktoarm terpolymers

Code	M_n (kDa)			Volume ratio (d)PS : PI : P2VP
	(d)PS	PI	P2VP	
SIV	10.6	11.2	44.9	0.17 : 0.20 : 0.63
dSIV	10.6	11.2	42.2	0.16 : 0.21 : 0.63

* based on densities of PS, dPS, PI, P2VP equal to 1.04, 1.14, 0.92, 1.14 g cm^{-3}, respectively.

To observe the bulk morphologies of protonated SIV and perdeuterated dSIV miktoarm terpolymers, the samples for SAXS and SANS were thermally annealed at 190 °C under vacuum for 4 days and then slowly cooled to room temperature. SAXS was performed on a Ganesha SAXS-LAB using Cu Kα radiation (λ = 0.154 nm). The sample-to-detector distance was 1041 mm, and the X-ray beam area was 0.04 mm^2. SANS measurements were conducted on the EQ-SANS instrument at the Spallation Neutron Source at the Oak Ridge National Laboratory.[38] The SANS intensities were obtained by using neutrons with wavelengths of 10.11 Å < λ < 13.2 Å at a sample-to-detector distances of 4 m. For TEM measurements, the thin sections (~50 nm) of microtomed samples were stained for 2–4 h with iodine (I_2) vapor and/or for 4 h with osmium tetroxide (OsO_4) vapor to distinguish each block and they were measured using a JEOL 2000FX TEM operated at an accelerating voltage of 200 kV.

Self-Consistent Field Theory (SCFT). Details of the SCFT calculations for ABC miktoarm terpolymers have been reported in the literature.[12,13,39-42] Here, we briefly describe the SCFT and model parameters for SIV with dSIV. After defining Hamiltonian for the ABC

miktoarms by including the Wiener measure for chain stretching and repulsive short-ranged interactions among different kinds of segments, we used standard field theoretical transformations to construct a field theory. Standard saddle-point approximation on the field theory yielded non-linear SCFT equations which were solved iteratively for equilibrium volume fraction distribution of the three different components. Polyswift ++[43] was used for all the SCFT calculations in this work, which uses the pseudo-spectral method[44] for solving modified diffusion equations appearing at the saddle-point. In writing the Hamiltonian, three arms of the ABC miktoarm terpolymer were represented by Gaussian chains, each of length $N_i l_i$, where i is the index of the block (i = 1, 2, 3 represents S, I, and V, respectively), N_i and l_i stand for the number and length of segments in i_{th} block, respectively. The interactions between dissimilar polymer segments were defined by Flory-Huggins interaction terms χ_{ij}, where i and j represent indices of the blocks. All the polymer segments were assumed to be of the same segment length ($l_1 = l_2 = l_3 = l$), where $l = v^{1/3}$ ($v = (v_S v_I v_V)^{1/3}$) is the geometric mean of the molar volume of the polymer segments. The molar volumes of the different components were obtained by dividing the polymer density by their respective monomer molar mass. In particular, the bulk densities of dPS, PI, and P2VP were taken to be 1.14, 0.92, and 1.14 g cm^{-3}, respectively and the monomer molar masses for dS, I, and V are 112.2, 68.12, and 105.14 g mol^{-1}, respectively. For the SCFT calculations, spatial dimensions of the simulation boxes were scaled with respect to $R_{go} = l(N/6)^{1/2}$, where $N = \sum_{i=1}^{3} N_i$ was defined as the ratio of total molar volume of the block co-polymer to the mean molar volume of the segments (v). The chain fraction, defined as $f_i = N_i/N$, was assumed to be the volume fraction of the respective component. The interaction parameters were obtained from the studies reported in the literature. However, we are not aware of any report discussing interactions of deuterated styrene with isoprene and 2-vinylpyridine and effects of deuteration

on short-range interactions were assumed to be negligible. One of the main criteria for observing the experimental morphology is: $\chi_{SI} \sim \chi_{VS} << \chi_{IV}$. The deuteration of polystyrene may influence χ_{SI} and χ_{SV} to some extent but the difference is inconsequential relative to the absolute value. Hence this assumption seems reasonable for such system. Specifically, we used the interaction parameters for hydrogenated styrene, which were reported to be $\chi_{SI} = 0.0685$[45] and $\chi_{VS} = 0.0867$[46] at 190 °C (annealing temperature for the samples). Also, χ_{IV} was reported to be about eight times that of χ_{SI} based on solubility parameter estimation.[47] For modeling purposes, we assumed $\chi_{IV} = k\chi_{SI}$ and k was varied to explore the morphological changes as a function of the relative interaction strength. Very high values of k were not explored as it becomes numerically challenging. The calculations were performed in both two and three dimensions. The grid size was varied between $0.1R_{go}$ and $0.15R_{go}$, and the number of grid points was varied between 64 x 64 and 128 x 128, for the simulations executed in two dimensions. For the simulations executed in three dimensions, the grid size was set at $0.1R_{go}$ and $0.15R_{go}$, and the number of grid points was taken to be 96 x 96 x 16. Variations of the grid sizes were done to ensure that the issue of incommensurability between period of the microphase separated morphologies and size of the simulation box doesn't affect the SCFT results. Simulations in three dimensions were executed to ensure that the morphology observed in the simulations ran in two dimensions simply translates in the third direction as well. Morphologies with the lowest free energy per chain (with respect to a completely disordered system) were reported here (see Table S1 in the SI). For attaining morphology with the lowest free energy, the following steps were taken. (a) Zone annealing was performed, wherein locally the structure was relaxed by decreasing the χN values to arbitrarily low values (typically much below the order-disorder limit of χN). This cycle of local relaxation was repeated throughout the simulation box and for a large number of iterations until the structure in the simulation box was relaxed.[48] (b) Different initial

conditions were used for the simulation: disordered, three different lamellar like structures (3-lamellar (LAM-3), alternate lamellar (ALT.LAM), cylinder in undulated lamellar (CYLULAM)) (Figure S3), five different tiling structures ([12.6.4], [6.6.6], [8.8.4], [8.6.6.; 8.6.4], [10.6.6; 8.8.4])[12,29] and core shell hexagonally packed structure. (c) The box dimensions were varied to avoid the artifacts due to buildup of stresses resulting from incommensurability of repeat distance of the morphologies and the box sizes and ensuring that (d) the morphology was retained in three dimensions. A summary of the model parameters used for the simulations is given in Table 2.

Table 2. The parameters for dSIV miktoarm melts. Here, $N = \sum_{j=1}^{3} N_j$, f represents the chain fraction of the respective component and χ_{ij} represents the pairwise interaction parameter between different components.

N	f_{dPS}	f_{PI}	f_{P2VP}	$\chi_{SI}N$	$\chi_{VS}N$	$\chi_{IV}N^*$
668	0.16	0.21	0.63	45.7	57.9	45.7–160.0

* $\chi_{IV}N$ is varied over a range of $1.0\chi_{SI}N \leq \chi_{IV}N \leq 3.5\chi_{SI}N$

Static Structure Factor from Equilibrium Volume Distribution Profiles. The equilibrium volume distribution profiles, obtained from the SCFT calculations, were used to calculate the scattering profiles of the bulk samples for comparison to the experimental profiles. The volumetric mean of the neutron scattering length density (NSLD) at every grid point was used to construct the spatial distribution of the scattering length density (SLD), i.e., $\rho(x,y) = \sum_{i=1}^{3} SLD_i \phi_i(x,y)$, where SLD_i and $\phi_i(x,y)$ represent the SLD and volume fraction of i at location (x,y). The SLDs of the hydrogenated and deuterated components are given in Table 3.[49,50] A FFTW (Fastest Fourier Transform in the West) library was used for the Fourier transformation, $\mathcal{F}$, of $\rho(x, y)$. $\mathcal{F}(q_x, q_y)$ = Fourier Transform $\{\rho(x, y)\}$, where $q_x = 2\pi m/L_x$ and $q_y = 2\pi m/L_y$ are the x and y components of the scattering vector q, L_x and L_y

represent the length of the simulation box in the x and y directions, respectively.[51] m and n are integers ranging from 0 to $N_x/2$ and 0 to $N_y/2$, respectively, where N_x and N_y are the number of grids in x and y directions, respectively. The static structure factor S(q) was obtained as a function of the scalar wave vector $q = (q_x^2+q_y^2)^{1/2}$ using its definition $S(q) = <\mathcal{F}(q)\,\mathcal{F}(-q)>/(N_xN_y)$, where the angular bracket <> represents azimuthally averaged value of S(q).

Table 3. Electron and neutron scattering length densities (SLDs) of different components, where d represents fully deuterated component.[49,50]

	Electron SLD ($\times10^{-6}$ Å^{-2})	**Neutron SLD** ($\times10^{-6}$ Å^{-2})
dPS	10.4	6.47
dPI	8.7	7.05
dP2VP	10.3	6.72
PS	9.5	1.39
PI	8.6	0.27
P2VP	10.3	1.94

RESULTS AND DISCUSSION

We synthesized the PS-PI-P2VP (SIV) miktoarm terpolymer and its analog with deuterated PS (dSIV) by living anionic polymerization. Both the SIV and dSIV have fairly similar compositions and total molar masses (Table 1). The samples were thermally annealed at 190 °C for 4 days in high vacuum (~0.01 mbar) to avoid the degradation, specifically crosslinking, from oxidation.

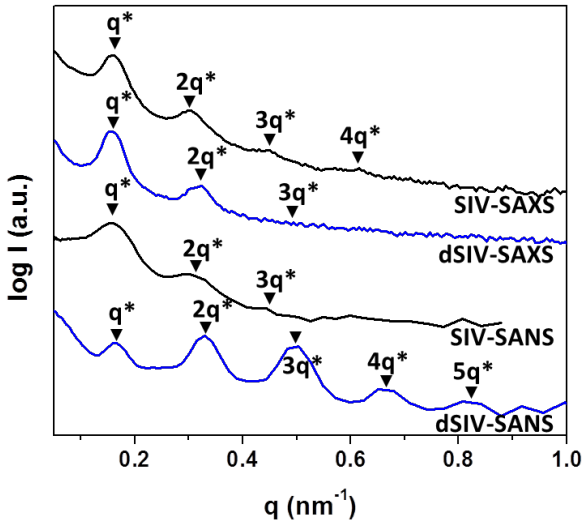

Figure 1. Small angle X-ray and neutron scattering (SAXS and SANS) profiles for SIV (black line) and dSIV (blue line) in the bulk after thermal annealing at 190 °C for 4 days. The scattering profiles are shifted vertically for clarity. The inverted triangles indicate the position of the primary (q^*) and higher order reflections.

The SAXS profiles of the SIV and dSIV miktoarm terpolymers as a function of the scattering vector (q) were measured at room temperature after thermal annealing as shown in Figure 1. For the fully protonated SIV, a highly-ordered lamellar microdomain morphology was observed with $L_0 = 2\pi/q^*$ of 39.6 nm ($q^* = 0.159$ nm^{-1}), as evidenced by the multiple higher order reflections at scattering vector ratios of 1:2:3:4 relative to the primary reflection

(q^*). The dSIV miktoarm terpolymer having the same molar mass as SIV also shows a lamellar morphology with a similar L_0 of 40.5 nm (q^* = 0.155 nm^{-1}). Since the X-ray scattering results from spatial variations in the electron density, (P2VP (3.65 x $10^{23}e/cm^3$), PI (3.09 x $10^{23}e/cm^3$), and PS (3.40 x $10^{23}e/cm^3$)), the scattering intensity is proportional to the square of the differences in the electron densities of the three blocks, $(\rho_{e,PS}- \rho_{e,PI})^2$, $(\rho_{e,PS}- \rho_{e,P2VP})^2$, and $(\rho_{e,PI}- \rho_{e,P2VP})^2$, which are 0.96 x $10^{45}(e/cm^3)^2$, 0.62 x $10^{45}(e/cm^3)^2$, and 1.30 x $10^{45}(e/cm^3)^2$, respectively. So, while the dominant contribution to the SAXS will arise from the contrast between PS and PI or P2VP and PI, there will still be a contribution from the PS and P2VP contrast, though the latter will be much less. Nonetheless, there will be ambiguity in the interpretation of the SAXS data.

SANS measurements were performed using the EQ-SANS instrument at the Spallation Neutron Source at Oak Ridge National Laboratory, where the PS block of the terpolymer was perdeuterated. In Figure 1, the SANS profiles for SIV and dSIV miktoarm terpolymers after thermal annealing are also shown. For SIV, a primary scattering peak at the same position as SAXS is seen along with higher order reflections ($2q^*$ and $3q^*$) corresponding to a lamellar morphology. The reflections are weaker and less well-defined than the SAXS reflections, since the contrast arises primarily from the mass density differences between the components. The NSLD of PI is 0.27×10^{-6} $Å^{-2}$, in comparison to the NSLD of P2VP of 1.94×10^{-6} $Å^{-2}$ and PS of 1.39×10^{-6} $Å^{-2}$, which is similar to the trend in the electron densities and, as such, the SAXS and SANS results provide essentially the same information. Both the SAXS and the SANS results show that the scattering intensity diminishes with increasing angle. By labeling only the styrene block with deuterium, the NSLD of the PS increases to 6.47 x 10^{-6} A^{-2} and a significantly distinct scattering profile is observed. Multiple higher order reflections, up to $5q^*$, are seen, indicative of a highly ordered

lamellar structure with an L_0 of 38.3 nm (q^* = 0.164 nm^{-1}). In addition, second and third order reflections are more intense than the primary reflection, suggesting either an unusual symmetry is causing a variation in the intensity of the reflections or that scattering arising from a different length scale, essentially one-half and one-third the length scale of the length scale of the primary reflection, is incoherently adding to the scattering from the lamellar microdomain morphology. These SANS results will be discussed more fully in light of our SCFT calculations to identify the morphology (see below). The persistence in the SANS up to a fifth order clearly shows a highly regular stacking of the lamellar microdomains and, therefore, the dissipation in the SAXS and SANS for the SIV and the SAXS for the dSIV indicate that a diffuse haze boundary or an apparent diffuse phase boundary is giving rise to the loss in intensity at higher scattering vectors.

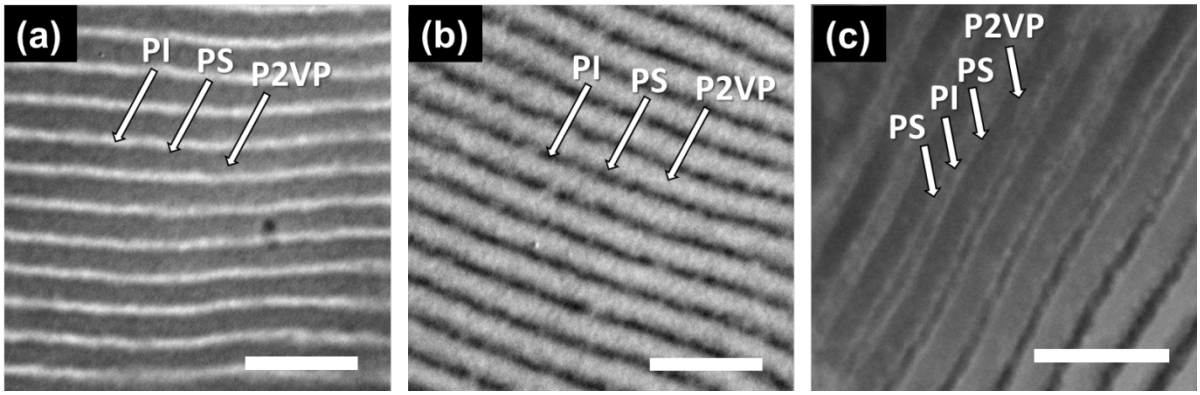

Figure 2. TEM images of dSIV miktoarm terpolymers with different staining reagents; (a) I_2 (dark P2VP / bright PS and PI), (b) OsO_4 (dark PI / bright PS and P2VP), (c) I_2 and OsO_4 (dark PI and P2VP / bright PS) staining. The scale bar is 100 nm.

TEM images of the dSIV are shown in Figure 2. Using different staining reagents, each microdomain can be distinguished since the P2VP microdomain in the lamellar structure of dSIV is black or white depending on whether it is stained by I_2 (Figure 2a) or OsO_4, respectively (Figure 2b). The widths of the lamellae microdomains of P2VP to the other

lamellae microdomain are 63:37 which is consistent with the value based on the volume fractions of the components (Φ_{PS} : Φ_{PI} : Φ_{P2VP} = 16 : 21 : 63). To distinguish PS from PI and P2VP, both I_2 and OsO_4 staining were used to render the P2VP and PI phase dark and PS phase bright, as shown in Figure 2c. Consequently, a micrograph of the three-phase four-layer lamellar microdomain morphology for dSIV was obtained. The dark PI lamellae are embedded in a PS matrix, resulting in a sequence of PS-PI-PS-P2VP layers. It is also evident that the very non-favorable contacts between the PI and P2VP domains are minimized by the intervening PS layer, since $\chi_{SI} \sim \chi_{VS} << \chi_{IV}$.

In terms of composition and total molar mass, both the SIV and dSIV miktoarm terpolymers are quite similar but the SAXS and SANS profiles for dSIV are qualitatively distinct from those for SIV. To better understand and characterize the morphology, we used the SCFT based calculation, where we only considered the dSIV miktoarm polymer and the details of the SCFT parameters are presented in Table 2. The volume fraction and total number of segments were mapped directly from the experimental parameters, whereas some of the interaction parameters (χ_{SI},χ_{VS}) were obtained from the literature. The only unknown parameter for the system, χ_{IV}, was systematically varied to obtain different equilibrium morphologies to compare against experimental SAXS, SANS, and TEM results. The equilibrium volume fractions of the three different components of dSIV were obtained as a function of relative strength of the interaction between PI-P2VP over PS-PI (i.e., $k = \chi_{IV}/\chi_{SI}$ with fixed $\chi_{SI} = 0.0685$) and results are shown in Figure 3. In the simplified summary column, the maximum volume fraction of the component at any grid point was used to color that point. The detailed volume fractions of each component (left side of Figure 3) show slightly diffuse interfaces unlike the sharp interfaces from the simplified three-color representation. The detailed information about the free energy between the competing structures for a given k and

the three dimensional images are presented in the SI (Section SI-2).

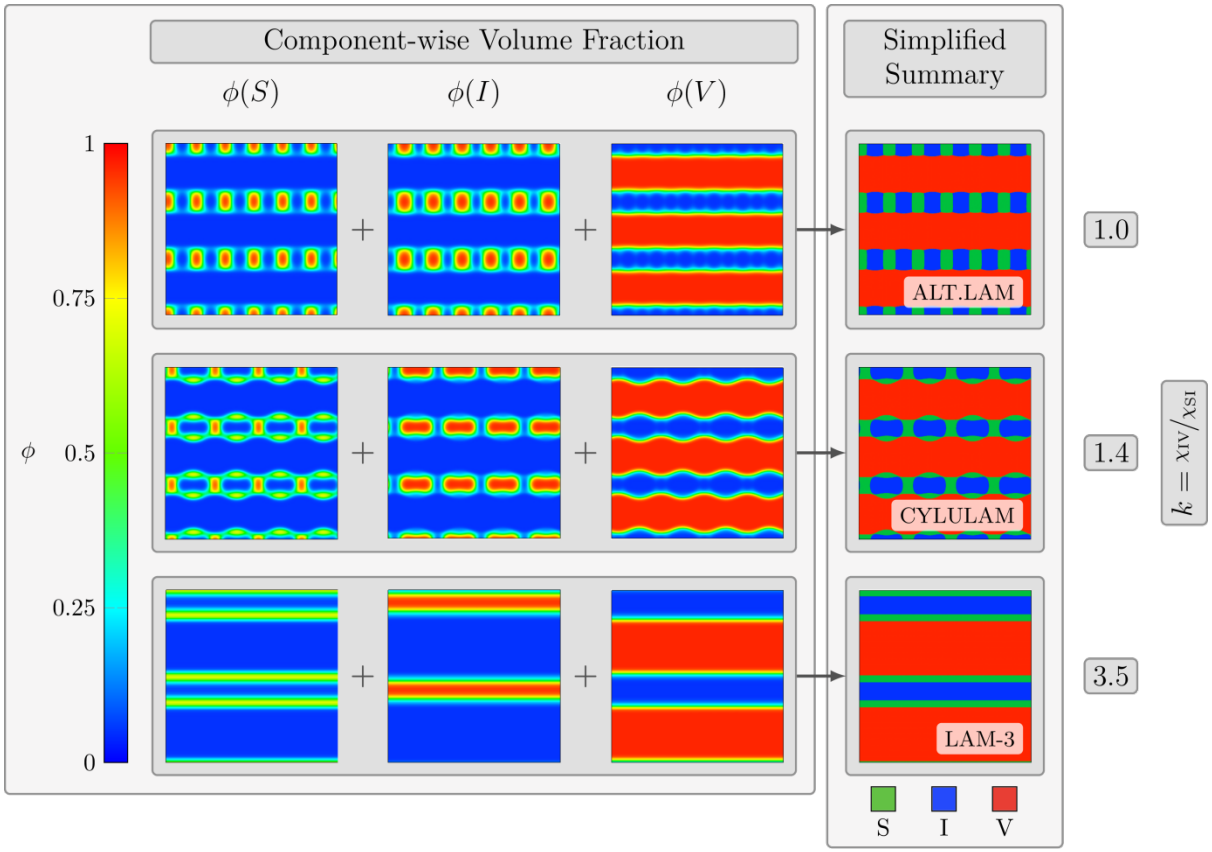

Figure 3. . Equilibrium morphologies of the dSIV miktoarm terpolymer obtained using the SCFT. The relative interaction strength parameters were varied so that $k = \chi_{IV}/\chi_{SI}$ = 1.0, 1.4 and 3.5 while χ_{SI} was fixed at 0.0685. In the simplified summary, the color-codes represent maximum volume fraction at a grid point and are: green-dPS, blue-PI, and red-P2VP. The volume fraction profiles are also presented along with the color bar for the volume fraction for reference. The morphology transitions from (a) alternate lamellar (ALT.LAM) at k = 1.0 to cylinder in undulated lamellar (CYLULAM) at k = 1.4 and finally to 3-lamellar (LAM-3) structure for k = 3.5.

The equilibrium morphology of the dSIV miktoarm terpolymer transitions from an alternate lamellar (ALT.LAM) morphology at k = 1.0 to cylinder in undulated lamellar

(CYLULAM) morphology at k = 1.4 and then into 3-lamellar (LAM-3) morphology as the strength of the relative interaction parameter k becomes equal or greater than 2.0 (only shown for k = 3.5 in Figure 3). When the repulsive interactions between PI and P2VP are low (i.e., k = 1.0), PI is exposed to P2VP in the ALT.LAM structure. By gradually increasing the repulsions between PI and P2VP, PS mitigates these unfavorable interactions, leading ultimately to the LAM-3 morphology where a layer of PS separates the layers of PI and P2VP. All of these three structures have been reported in previous studies for ABC miktoarm terpolymers.[12,15,17,18] Since χ_{IV} is the unknown parameter, by comparison of the simulation results to the TEM results and semi-quantitatively to the SAXS and SANS profiles, χ_{IV} can be estimated and compared to that derived from the solubility parameter ($\chi_{IV}/\chi_{SI} \sim 8$).[47] The k value reported in the literature provides an estimate and it is numerically difficult to simulate copolymers using such a high value of k due to the presence of very sharp interfaces in such simulations. Computed scattering profiles from the three different morphologies, ALT.LAM (k = 1.0), CYLULAM (k = 1.4), and LAM-3 (k = 3.5), were compared to the SAXS and SANS profiles of dSIV miktoarm terpolymer. For direct comparisons of the SCFT-based scattering profiles with SAXS and SANS, the following steps were applied:

1. Location of the primary peak in scattering curves for block polymer melts gives characteristic length scale of microphase separation. In order to reproduce the same length scale in the SCFT calculations, one can either vary conformational characteristics of the block polymer chains such as the Gaussian radius of gyration (R_{go}) or the interaction parameters χ_{ij}. For the ABC miktoarm terpolymer melts, we compared the SCFT based scattering curves with experiments by rescaling R_{go} while converting dimensionless wave vector $q^* = q\,R_{go}$ (Figure S5 and S7) into q (in the units of nm^{-1}). Specifically, q^* was divided by R_{go1} instead of $R_{go,}$ where R_{go1} was obtained by fitting the primary peak position in the

computed scattering curves (q^*) to the primary peak position (q) in the experimental SAXS and SANS profiles. An alternative approach of varying the interaction parameters to match the primary peak was not attempted due to the lack of quantitative data on the parameters. In retrospect, one can compute the total number of Kuhn segments (N_k) and the effective Kuhn segment length (l_k) for a given value of the asymmetry parameter k, which can represent the specific experimental system studied here. For such computations, we used the definition $R_{gol} = l_k (N_k/6)^{1/2}$ and equate the contour length of the new model against the model presented in Table 2 (i.e., $l_k N_k = lN$). Solving these two algebraic equations, l_k and N_k were obtained (Table S2). The calculated l_k were reasonable as they lie within the range of Kuhn segment lengths of the individual components (the Kuhn segment length (l) for PS, PI, and P2VP are 1.8, 0.9, and 1.8 nm, respectively).[52] This analysis highlights sensitivity of the scattering curves to the choice of the Kuhn segment length.

2. After obtaining the dimensional form of q, the model data is convoluted with a one-dimensional Gaussian function ($\boldsymbol{G(x) = (2\pi\sigma^2)^{-\frac{1}{2}} e^{-\frac{x^2}{2\sigma^2}}}$, where σ is the standard deviation). The specified SAXS and SANS instrument resolution functions were used as a standard deviation. The standard deviation for SAXS was 0.01356 nm^{-1} and the q-dependent standard deviation for the SANS instrument is provided in the SI (Figure S8).

3. The magnitude of the convoluted data was then scaled such that the primary peak in the model magnitude matched with that in the SAXS and SANS magnitude.

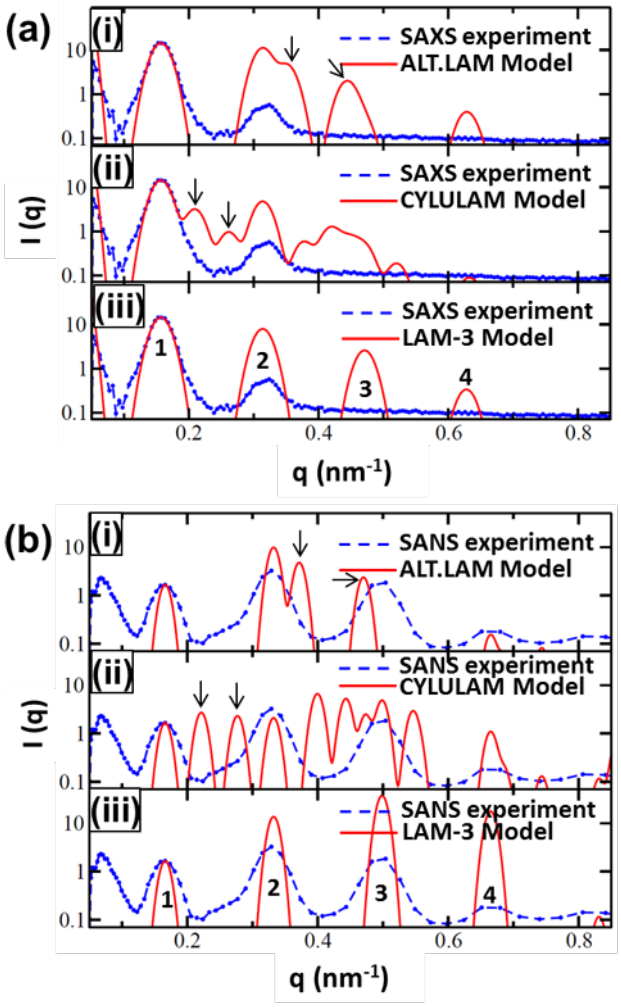

Figure 4. Comparison of computed scattering profiles with the experimental SAXS and SANS profiles of dSIV miktoarm terpolymer by taking into consideration the SLD of different components (Table 3) followed by post processing (Section SI-3). (i), (ii), and (iii) in both (a) and (b) correspond to three different morphologies, namely; (i) ALT.LAM (k = 1.0), (ii) CYLULAM (k = 1.4), and (iii) LAM-3 (k = 3.5). LAM-3 structure represented both the SAXS and SANS profiles almost quantitatively. The arrows in ALT.LAM and CYLULAM scattering profiles indicate the position of the first two secondary peaks.

As shown in Figure 4a, it is challenging to determine which model represented the SAXS data best, given that only two multiple order reflections were observed and the intensity of third order reflection was too small. The distinguishing feature between LAM-3

structure and other two structures was the presence of distinct peaks corresponding to the secondary length scale in ALT.LAM and CYLULAM structure. The first two secondary model peaks are indicated using arrows in Figure 4 for both the ALT.LAM and CYLULAM structures. However, those computed peaks appeared only as shoulders which could be missed in the experiment due to instrument resolution and incoherent background, especially for the case of ALT.LAM structure. Whereas, in the SANS results (Figure 4b), computed peaks corresponding to the secondary length scales appeared magnified for ALT.LAM and CYLULAM. Out of the three models, the LAM-3 model represented the SANS scattering profile the best. The peaks were observed at 1:2:3:4:5 and the peak positions exactly matched those observed in SANS. Moreover, the higher order reflections were more intense than the primary reflection, qualitatively similar to the SANS profile. Hence, the LAM-3 morphology was found to be the most appropriate morphology for the dSIV miktoarm terpolymer based on the detailed SCFT studies.

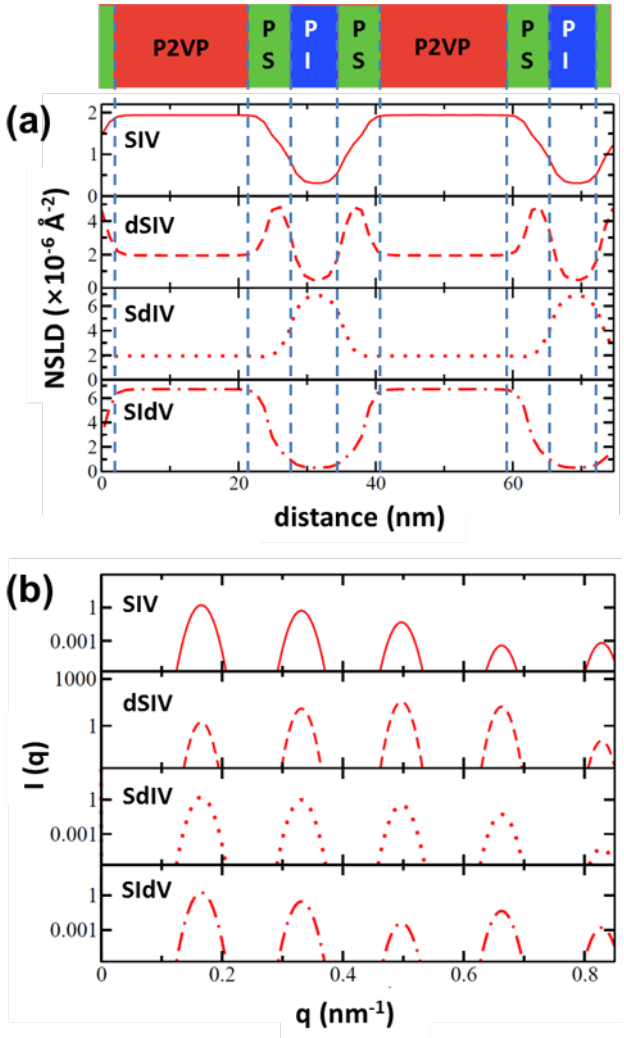

Figure 5. (a) One-dimensional NSLD of LAM-3 structure and their (b) corresponding computed SANS for different deuteration labeling. Only when PS is deuterated, the computed SANS profile shows the unique feature of smaller primary reflection than the higher order reflections.

Scattering calculations based on the SCFT were repeated for k = 3.5 by deuterating different components of SIV, one component at a time. For the LAM-3 structure, the two-dimensional SLD can be simplified to a one-dimensional SLD profile and are shown in Figure 5a. Only when PS is deuterated, the computed SANS profile (Figure 5b) showed qualitatively similar behavior as seen in experiments. In other cases, the SANS profiles exhibited primary reflection to be larger in magnitude than the higher order reflections.

Closer examination of the SLD profiles indicated that only for the case of dSIV, the PS domain shows distinct contrast relative to PI and P2VP. For the other cases, the SLD appears the smooth transition from the P2VP rich region to the PI rich region. This distinct feature of the SLD of dSIV is translated into anomalous behavior in the scattering profile. It should be pointed out that variations of the SLD due to deuteration can explain scattering pattern for LAM-3 morphology. In practice, the deuteration can affect not only SLD but also the interaction parameters resulting from molar volume changes and polarizability.[53,54] However, we expect those changes due to deuteration on the interactions to affect location of the peaks by affecting sizes of microphase separated domains with very small effects on the shapes of the scattering curves.

There have been several studies on the morphology of SIV miktoarm terpolymers having approximately similar compositions. Matsushita and coworkers have reported ALT.LAM structure with composition of S:I:V = 0.2:0.2:0.6.[35] The CYLULAM structure was reported by Chernyy and coworkers for a similar composition, S:I:V=0.17:0.17:0.66.[36] It has been shown that composition, molar mass, and configuration of PI have significant effects on the morphology. The dSIV miktoarm terpolymer in this study is very similar to the sample (code: ISV-4) in a previous study.[36] Both used similar synthetic route, therefore both cases are expected to have the same configuration of PI (predominantly poly(*cis*-1,4-isoprene)). The total molar mass for both cases are also similar (dSIV: 64kDa, ISV-4: 71kDa). Closer examination of the composition shows that the volume ratio of PS and PI is slightly asymmetric in our case, 1:1.3, in comparison to the completely symmetric ratio (1:1) for ISV-4. Whereas, the volume ratio of PS and P2VP is equally asymmetric for both cases, 1:4.0 for dSIV and 1:3.9 for ISV-4. In fact, for a very wide range of PS *vs* P2VP volume ratio, 1:1.9 to 1:3.9, CYLULAM morphology was observed.[36]

Triggered by the slight asymmetry in the composition observed (discussed above), we investigated the effect of the volume of PS on the morphology of the dSIV by keeping the volume ratio of other two components fixed (Φ_I:Φ_V=1.3:4.0). Consequently, the volume fractions of the three components varied, but the other parameters, namely the three pairwise interaction parameters and the total number of segments, were held constant for these simulations. As shown in Figure 6, with a gradual increase in the volume of PS, the morphology changes from LAM-3 to CYLULAM. This transition occurs near the composition where the volumes of PS and PI are nearly the same (1:1.09). The LAM-3 structure is retained with a Φ_S:Φ_I of 1:1.3. The pairwise interaction parameter between the different components can explain the effect of the Φ_S on the morphology. Since PI and P2VP are highly incompatible, PS is placed at the interface of PI and P2VP to mediate nonfavorable interactions. Hence, with increase in the volume of PS, a CYLULAM morphology is found.

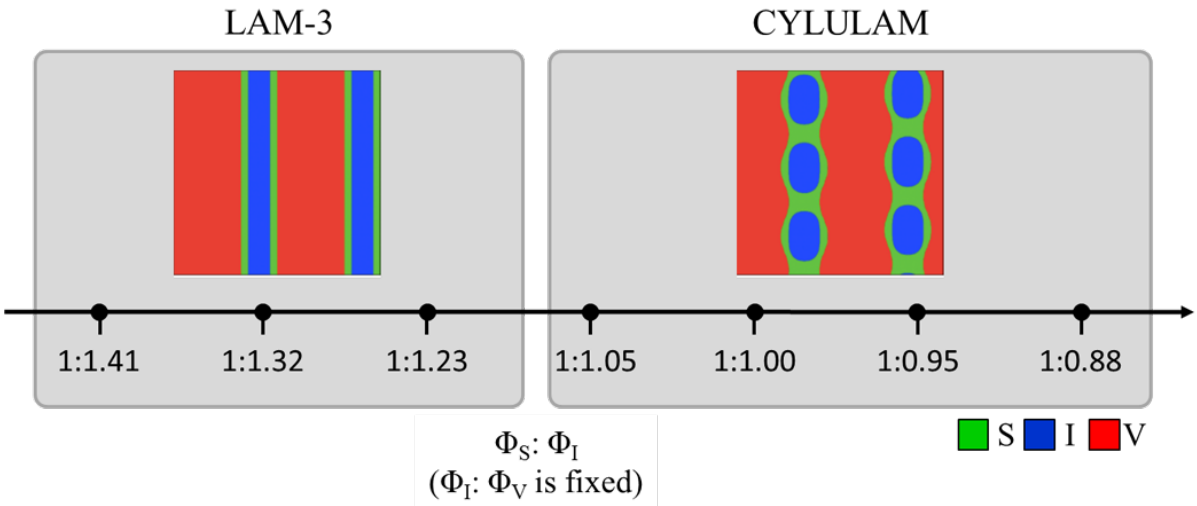

Figure 6. Effect of composition on the morphology of the SIV miktoarm terpolymer. The change in volume of PS is reflected in the volume fraction of Φ_S:Φ_I as shown in the pseudo *x*-axis. As the volume fraction of PS increases with corresponding decrease in the volume fraction of PI, the morphology changes from LAM-3 to CYLULAM. The color-codes (represents maximum volume fraction at a grid point) are: green-PS, blue-PI, and red-P2VP.

CONCLUSION

In summary, the LAM-3 structure has been realized from the self-assembly of SIV miktoarm terpolymer with a volume ratio of the blocks of 1:1.3:4.0. We investigated not only the local ordering by TEM, but the averaged structures by analyzing SAXS and SANS data simultaneously, taking advantage of the differences in the electron densities and NSLDs of the components. This structure was also generated by SCFT calculations based on the interaction strengths. The LAM-3 was found to be the most stable morphology for $\chi_{IV}/\chi_{SI} \geq 2$. Furthermore, LAM-3 exhibited a unique SANS scattering pattern when styrene was deuterated in which primary peak had lower intensity than the next two higher order peaks. Absence of peaks due to secondary length scales in the obtained experimental SAXS profiles and presence of higher order peaks of larger magnitude compared to the primary peak indicates that LAM-3 structure is indeed the observed structure in the experiments. This synergistic experiment and simulation study highlights the need to carefully examine the scattering from multicomponent block polymer melts.

ASSCOCIATED CONTENT

Supporting Information. Synthetic procedures, SCFT data, SANS instrument resolution functions. This material is available free of charge via the Internet at http://pubs.acs.org.

AUTHOR INFORMATION

Corresponding Author

*(T.P.R) E-mail: russell@mail.pse.umass.edu, Tel (413) 577-1516, Fax (413) 577-1510.

Notes

The authors declare no competing financial interest.

ACKNOWLEDGEMENT

This research was supported by the Laboratory Directed Research and Development Program of Oak Ridge National Laboratory, managed by UT-Battelle, LLC, for the U.S. Department of Energy (DOE). The Research at Oak Ridge National Laboratory's Spallation Neutron Source was sponsored by the Scientific User Facilities Division, Office of Basic Energy Sciences, U.S. DOE. A portion of this research was conducted at the Center for Nanophase Materials Sciences, which is a DOE Office of Science User Facility. BGS, RK, MG, KH, and WW acknowledge work performed at the Center for Nanophase Materials Science which is a U.S. DOE Office of Science User Facility. HK, DMY and TPR were supported by the Air Force Offices of Scientific Research under contract 16RT1602. MMLA and JPM were supported by the Laboratory Directed Research and Development, Technology Innovation Program of ORNL managed by UT-Battelle, LLC for the U.S. DOE.

References

[1] Kim, H.-C.; Park, S.-M.; Hinsberg, W. D. *Chem. Rev.* **2010**, 110, 146–177.

[2] Jeong, S.-J.; Kim, J. Y.; Kim, B. H.; Moon, H.-S.; Kim, S. O. Directed Self-Assembly of Block Copolymers for Next Generation Nanolithography. *Mater. Today* **2013**, 16, 468–476.

[3] Hawker, C. J.; Russell, T. P. Block Copolymer Lithography: Merging "Bottom-up" with "Top-Down" Processes. *MRS Bull.* **2005**, 30, 952–966.

[4] Koo, K.; Ahn, H.; Kim, S.W.; Ryu, D.Y.; Russell, T.P. Directed self-assembly of block copolymers in the extreme: guiding microdomains from the small to the large. *Soft Matter* **2013**, 9, 9059-9071.

[5] Phillip, W.A.; O'Neill, B.; Rodwogin, M.; Hillmyer, M.A.; Cussler, E.L. Self-assembled block copolymer thin films as water filtration membranes. *ACS Appl. Mater. Interfaces* **2010**, 2, 847-853.

[6] Pitsikalis, M.; Pispas, S.; Mays, J.W.; Hadjichristidis, N. *Nonlinear block copolymer architectures. In Blockcopolymers-Polyelectrolytes-Biodegradation*. Springer, Berlin, Heidelberg. 1998; 1-137

[7] Hadjichristidis, N.; Iatrou, H.; Pitsikalis, M.; Pispas, S.; Avgeropoulos, A. Linear and non-linear triblock terpolymers. Synthesis, self-assembly in selective solvents and in bulk. *Prog. Polym. Sci.* **2005**, 30, 725-782.

[8] Fujimoto, T.; Zhang, H.; Kazama, T.; Isono, Y.; Hasegawa, H.; Hashimoto, T. Preparation and characterization of novel star-shaped copolymers having three different branches. *Polymer* **1992**, 33, 2208-2213.

[9] Feng, H.; Lu, X.; Wang, W.; Kang, N.G.; Mays, J.W. Block copolymers: Synthesis, self-assembly, and applications. *Polymers*, **2017**, 9, 494.

[10] Okamoto, S.; Hasegawa, H.; Hashimoto, T.; Fujimoto, T.; Zhang, H.; Kazama, T.; Takano, A.; Isono, Y. Morphology of model three-component three-arm star-shaped copolymers. *Polymer* **1997**, 38, 5275-5281.

[11] Matsushita, Y.; Hayashida, K.; Dotera, T.; Takano, A. Kaleidoscopic morphologies from ABC star-shaped terpolymers. *J. Phys.: Condens. Matter* **2011**, 23, 284111.

[12] Zhang, G.; Qiu, F.; Zhang, H.; Yang, Y.; Shi, A.-C. SCFT study of tiling patterns in ABC star terpolymers. *Macromolecules* **2010,** 43, 2981-2989.

[13] Jiang, K.; Zhang, J.; Liang, Q. Self-Assembly of Asymmetrically Interacting ABC Star Triblock Copolymer Melts. *J. Phys. Chem. B* **2015**, 119, 14551-14562.

[14] Li, W.; Xu, Y.; Zhang, G.; Qiu, F.; Yang, Y.; Shi, A.-C. Real-space self-consistent mean-field theory study of ABC star triblock copolymers. *J. Chem. Phys.* **2010**, 133, 064904.

[15] Tang, P.; Qiu, F.; Zhang, H.; Yang, Y. Morphology and phase diagram of complex block copolymers: ABC linear triblock copolymers. *Phys. Rev. E* **2004**, 69, 031803.

[16] Huang, C.I.; Fang, H.K.; Lin, C.H. Morphological transition behavior of A B C star copolymers by varying the interaction parameters. *Phys. Rev. E* **2008**, 77, 031804.

[17] Kirkensgaard, J.J.; Pedersen, M.C.; Hyde, S.T. Tiling patterns from ABC star molecules: 3-colored foams?. Soft matter **2014**, 10, 7182-7194.

[18] Kirkensgaard, J.J.K. Striped networks and other hierarchical structures in A m B m C n (2 m+ n)-miktoarm star terpolymer melts. *Phys. Rev. E* **2012**, 85, 031802.

[19] Fujimoto, T.; Zhang, H.; Kazama, T.; Isono, Y.; Hasegawa, H.; Hashimoto, T. Preparation and characterization of novel star-shaped copolymers having three different branches. *Polymer* **1992**, 33, 2208-2213.

[20] Okamoto, S.; Hasegawa, H.; Hashimoto, T.; Fujimoto, T.; Zhang, H.; Kazama, T.; Takano, A.; Isono, Y. Morphology of model three-component three-arm star-shaped copolymers. *Polymer* **1997**, 38, 5275-5281.

[21] Sioula, S.; Hadjichristidis, N; Thomas, E.L. Novel 2-dimensionally periodic non-constant mean curvature morphologies of 3-miktoarm star terpolymers of styrene, isoprene, and methyl methacrylate. *Macromolecules* **1998**, 31, 5272-5277.

[22] Sioula, S.; Hadjichristidis, N.; Thomas, E.L. Direct evidence for confinement of junctions to lines in an 3 miktoarm star terpolymer microdomain structure. *Macromolecules* **1998**, 31, 8429-8432.

[23] Takano, A.; Wada, S.; Sato, S.; Araki, T.; Hirahara, K.; Kazama, T.; Kawahara, S.; Isono, Y.; Ohno, A.; Tanaka, N.; Matsushita, Y. Observation of cylinder-based microphase-separated structures from ABC star-shaped terpolymers investigated by electron computerized tomography. *Macromolecules* **2004**, 37, 9941-9946.

[24] Takano, A.; Kawashima, W.; Noro, A.; Isono, Y.; Tanaka, N.; Dotera, T.; Matsushita, Y. A mesoscopic Archimedean tiling having a new complexity in an ABC star polymer. *J. Polym. Sci. B* **2005**, 43, 2427-2432.

[25] Hayashida, K.; Kawashima, W.; Takano, A.; Shinohara, Y.; Amemiya, Y.; Nozue, Y.; Matsushita, Y. Archimedean tiling patterns of ABC star-shaped terpolymers studied by microbeam small-angle X-ray scattering. *Macromolecules* **2006**, 39, 4869-4872..

[26] Hayashida, K.; Takano, A.; Arai, S.; Shinohara, Y.; Amemiya, Y.; Matsushita, Y. Systematic transitions of tiling patterns formed by ABC star-shaped terpolymers. *Macromolecules* **2006**, 39, 9402-9408.

[27] Aissou, K.; Choi, H.K.; Nunns, A.; Manners, I.; Ross, C.A. Ordered nanoscale Archimedean tilings of a templated 3-miktoarm star terpolymer. *Nano lett*. **2013**, 13, 835-839.

[28] Choi, H.K.; Nunns, A.; Sun, X.Y.; Manners, I.; Ross, C.A. Thin film knitting pattern morphology from a miktoarm star terpolymer. *Adv. Mater.* **2014**, 26, 2474-2479.

[29] Chernyy, S.; Kirkensgaard, J.J.K.; Mahalik, J.P.; Kim, H.; Arras, M.M.; Kumar, R.; Sumpter, B.G.; Smith, G.S.; Mortensen, K.; Russell, T.P.; Almdal, K. Bulk and Surface Morphologies of ABC Miktoarm Star Terpolymers Composed of PDMS, PI, and PMMA Arms. *Macromolecules* **2018**, 51, 1041-1051.

[30] Ueda, K.; Dotera, T.; Gemma, T. Photonic band structure calculations of two-dimensional Archimedean tiling patterns. *Phys. Rev. B* **2007**, 75, 195122.

[31] Bohbot-Raviv, Y.; Wang, Z.G. Discovering new ordered phases of block copolymers. *Phys. Rev. Lett* **2000**, 85, 3428.

[32] Liu, M.; Li, W.; Qiu, F.; Shi, A.C. Theoretical study of phase behavior of frustrated ABC linear triblock copolymers. *Macromolecules* **2012**, 45, 9522-9530.

[33] Tyler, C.A.; Morse, D.C. Orthorhombic F d d d Network in Triblock and Diblock Copolymer Melts. *Phys. Rev. Lett* **2005**, 94, 208302.

[34] Li, W.; Qiu, F.; Shi, A.C. Emergence and stability of helical superstructures in ABC triblock copolymers. *Macromolecules* **2011**, 45, 503-509.

[35] Matsushita, Y.; Hayashida, K.; Dotera, T.; Takano, A. Kaleidoscopic morphologies from ABC star-shaped terpolymers. *J. Phys. Condens. Matter* **2011**, 23, 284111.

[36] Chernyy, S.; Mahalik, J.P.; Kumar, R; Kirkensgaard, J.J.K.; Arras, M.M.; Kim, H.; Schulte, L.; Ndoni, S.; Smith, G.S.; Mortensen, K.; Sumpter, B.G.; Russell, T.P.; Almdal, K. On the Morphological Behavior of ABC Miktoarm Stars Containing Poly(cis 1,4-isoprene), Poly(styrene) and Poly(2-vinylpyridine). *J. Polym. Sci. B* **2018**, DOI: 10.1002/polyb.24733

[37] Uhrig, D.; Mays, J.W. Experimental techniques in high-vacuum anionic polymerization. *J. Polym. Sci. A* **2005**, 43, 6179–6222.

[38] Zhao, J.K.; Gao, C.Y.; Liu, D. The extended Q-range small-angle neutron scattering diffractometer at the SNS. J. Appl. Cryst. **2010**, 43,1068-1077.

[39] Xu, W.; Jiang, K.; Zhang, P.; Shi, A.C. A strategy to explore stable and metastable

ordered phases of block copolymers. *J. Phys. Chem. B* **2013**, 117, 5296-5305.

[40] Arora, A.; Qin, J.; Morse, D.C.; Delaney, K.T.; Fredrickson, G.H.; Bates, F.S.; Dorfman, K.D. Broadly accessible self-consistent field theory for block polymer materials discovery. *Macromolecules* **2016**, 49, 4675-4690.

[41] Grason, G.M.; Kamien, R.D. Self-consistent field theory of multiply branched block copolymer melts. *Phys. Rev. E* **2005**, 71, 051801.

[42] Grason, G.M. The packing of soft materials: Molecular asymmetry, geometric frustration and optimal lattices in block copolymer melts. *Phys. Rep.* **2006**, 433, 1-64.

[43] https://www.txcorp.com

[44] Sides, S.W.; Fredrickson, G.H. Parallel algorithm for numerical self-consistent field theory simulations of block copolymer structure. *Polymer* **2003**, 44, 5859-5866.

[45] Khandpur, A.K.; Foerster, S.; Bates, F.S.; Hamley, I.W.; Ryan, A.J.; Bras, W.; Almdal, K.; Mortensen, K. Polyisoprene-polystyrene diblock copolymer phase diagram near the order-disorder transition. *Macromolecules* **1995**, 28, 8796-8806.

[46] Zha, W.; Han, C.D.; Lee, D.H.; Han, S.H.; Kim, J.K.; Kang, J.H.; Park, C. Origin of the Difference in Order– Disorder Transition Temperature between Polystyrene-block-poly (2-vinylpyridine) and Polystyrene-block-poly (4-vinylpyridine) Copolymers. *Macromolecules* **2007**, 40, 2109-2119.

[47] Funaki, Y.; Kumano, K.; Nakao, T.; Jinnai, H.; Yoshida, H.; Kimishima, K.; Tsutsumi, K.; Hirokawa, Y.; Hashimoto, T. Influence of casting solvents on microphase-separated structures of poly (2-vinylpyridine)-block-polyisoprene. *Polymer* **1999**, 40, 7147-7156.

[48] Mays, J.W.; Kumar, R.; Sides, S.W.; Goswami, M.; Sumpter, B.G.; Hong, K.; Wu, X.; Russell, T.P.; Gido, S.P.; Avgeropoulos, A.; Tsoukatos, T. Morphologies of poly (cyclohexadiene) diblock copolymers: Effect of conformational asymmetry. *Polymer* **2012**, 53, 5155-5162.

[49] Sivia, D.S. *Elementary scattering theory: for X-ray and neutron users*. Oxford University Press. 2011

[50] Rauch, H.; Waschkowski, W. 6 Neutron scattering lengths. *In Low Energy Neutrons and their Interaction with Nuclei and Matter.* Springer, Berlin, Heidelberg. 2000; 1-29

[51] Frigo, M. A fast Fourier transform compiler. *Acm sigplan notices. ACM* **1999**, 34, 169-180.

[52] Rubinstein, M.; Colby, R.H. Polymer physics, Oxford university: New York, 2003; Vol.

23.
[53] Buckingham, A.D.; Hentschel, H.G.E. Partial miscibility of liquid mixtures of protonated and deuterated high polymers. *J. Polymer Sci.: Polymer Phys. Ed.* **1980**, 18, 853-861.
[54] Bates, F.S.; Wignall, G.T.; Koehler, W.C. Critical behavior of binary liquid mixtures of deuterated and protonated polymers. *Phys. Rev. Lett*, **1985**, 55, 2425.

for Table of Contents use only

Studies on the 3-Lamellar Morphology of Miktoarm Terpolymers

Hyeyoung Kim[1], Matthias M L Arras[2], J. P. Mahalik[3,4,5], Weiyu Wang[3], Duk Man Yu[1], Sergey Chernyy[6], Monojoy Goswami[3,4], Rajeev Kumar[3,4,5], Bobby G. Sumpter[3,4], Kunlun Hong[3], Gregory S. Smith[2], and Thomas P. Russell[1,7*]